ELSEVIER

Catalysis Today 74 (2002) 145–155

CATALYSIS TODAY

www.elsevier.com/locate/cattod

Methane decomposition to carbon nanotubes and hydrogen on an alumina supported nickel aerogel catalyst

Lingyu Piao [a], Yongdan Li [a,*], Jiuling Chen [a], Liu Chang [a], Jerry Y.S. Lin [a,b]

[a] *Department of Catalysis Science and Technology, State Key Lab of C1 Chemical Technology, School of Chemical Engineering, Tianjin University, Tianjin 300072, China*

[b] *Department of Chemical Engineering, University of Cincinnati, ML-171 Cincinnati, OH 45221-0171, USA*

Abstract

An alumina supported nickel aerogel catalyst was prepared by the sol–gel method and used in the catalytic decomposition of methane. An in situ thermal balance reactor was employed in the study of the reaction. A number of catalysts prepared by the same procedure with different nickel to aluminum ratio were tested. It has been observed that the catalyst oxide precursor has a $NiAl_2O_4$-like structure. The amount of the carbon nanotubes (CNTs) formed before the deactivation of the catalyst increases with the nickel content in the catalyst. CNTs grow in 450–700 °C. TEM micrographs show that the CNTs are curved, with diameters in the range of 10–20 nm. Both the reaction and catalyst reduction conditions have strong influences on the morphology of the CNTs and on the reaction behavior.

Keywords: Catalytic decomposition of methane; Carbon nanotubes; Sol–gel; Aerogel; Nickel catalyst; Morphology

1. Introduction

Since the publication of Iijima in 1991 [1], carbon nanotubes (CNTs) have been a category of the most actively investigated materials in many fields. Their outstanding chemical and physical properties and their potential applications in many fields have attracted researchers' interests [2–11]. However, the lack of materials in sufficient quantity limited the research on their properties and applications. These materials are often prepared by the methods of arc-discharge (ADE) [2,3,12,13] and laser beam evaporation (LBE) of graphite [14,15] and chemical vapor deposition (CVD) of carbon through catalytic decomposition of hydrocarbons [4,5,16–20]. Transition metals are used as catalysts during the ADE to favor the formation of the single-walled nanotubes [21–27]. The LBE method also uses transition metal as catalyst and can produce single-walled CNTs with a yield of more than 70% [28,29]. The ADE and LBE methods are however difficult to be scaled up.

CVD method has been used for preparation of multi-walled CNTs, and reported to have a high yield [30]. Several mechanisms have been proposed for the formation of tubular carbon material by this method. It has been postulated that the metal particles are active for nanotube nucleation and growth only if they are sufficiently small ($\leq$20 nm) [31–34]. Su et al. [35] reported that single-walled tubes were obtained using an alumina aerogel supported Fe/Mo catalyst. They prepared the catalyst using metal alkoxides (aluminum tri-sec-butoxide and $MoO_2(acac)_2$) and CO_2 supercritical drying.

* Corresponding author. Tel.: +86-22-2740-5613; fax: +86-22-2740-5243.
E-mail address: ydli@tju.edu.cn (Y. Li).

0920-5861/02/$ – see front matter
PII: S0920-5861(01)00540-5

Methane decomposition reaction (MDR) was commercialized for the production of ink carbon and hydrogen without employing a catalyst in the past [36,37]. In two recent reviews [38,39], this process was recommended as the most economical process for hydrogen production due to its low energy input. Recently, we proposed a concept of simultaneous production of carbon-monoxide-free hydrogen and nanocarbon materials [5]. Development of various technologies for the production of CO-free hydrogen has received increasing interest in scientific community due to recent progress in the low temperature fuel cells which cannot tolerate CO in the fuel. Many researchers [40–46] believe that the MDR method is a better route than steam reforming for production of hydrogen for fuel cell applications. Recently, we conducted MDR on an alumina supported nickel aerogel catalyst with emphasis on production of high quality carbon. The catalyst was prepared by the sol–gel method with supercritical extraction of the solvent. The results of our recent study are reported here.

2. Experimental

2.1. Catalyst preparation

The catalysts were prepared using a sol–gel technique with supercritical drying. The sol–gel preparation was carried out at room temperature. $Al(OH)_3$ sol was prepared by a dropwise addition of ammonia liquor (1.5 M) into an $Al(NO_3)_3$ solution (0.2 M) under vigorous stirring. The pH of the solution was around 7.8 at the end of the addition. Then a $Ni(NO_3)_2$ solution (0.2 M) and the ammonia liquor were added dropwise simultaneously to the $Al(OH)_3$ sol under vigorous stirring. The pH of the solution was controlled at around 9.3 during the addition. The gel obtained was then aged for about 3 h under stirring. In the last step, the water in the gel was replaced by ethanol until the ratio of water to ethanol was lower than 5% (analyzed by a GC).

Drying of the material was carried out under the supercritical condition of ethanol. Some wet gel with some ethanol was placed in a sealed 330 ml high-pressure container. Then the air in the container was quenched by nitrogen. The container was heated up to above the critical temperature of ethanol (here 260 °C). The pressure in the container increased to above the critical pressure (here 75 bar) at the same time. The system was held at this condition for 30 min. Then the pressure was released slowly while the temperature was kept constant. Finally, the temperature was lowered to ambient under nitrogen flow. The material formed is a typical aerogel, with very low density. This powder was then calcined at different temperatures. Table 1 lists the composition and preparation conditions of the catalysts used in this work.

Table 1
Samples used in this work

Samples	Ratio Ni^{2+}/Al^{3+} in the sample	Calcination temperature (°C) and time (h)
Q1	$Ni^{2+}:Al^{3+} = 1:9$	300, 400, 500, 600; 8
Q2	$Ni^{2+}:Al^{3+} = 2:9$	300, 400, 500, 600; 8
Q3	$Ni^{2+}:Al^{3+} = 3:9$	300, 400, 500, 600, 700; 8

2.2. Characterization of materials

A D/MAX-2038 X-ray diffractometer with Fe Kα was used to measure the XRD profiles of the catalysts. A JEM-100CX II TEM was used to obtain the micrographs of the samples. TPR was carried out in a tubular quartz reactor of 8 mm in diameter, at a heating rate of 10 °C/min. The amount of catalyst used in TPR was 100 mg and the gas flow was 8 vol.% H_2–N_2 mixture at a total flow rate of 40 ml/min (STP). BET surface area of the aerogel powder was measured on a CHEMBET 3000 using 60 mg sample, with N_2 adsorption method.

2.3. CNT growth

The reaction was carried out at atmospheric pressure in an in situ thermobalance (TB) reactor of 20 mm in diameter and 160 mm in length, located in a vertical furnace. Three milligram calcined catalyst was placed in a ϕ12 mm × 12 mm quartz basket hanging in the middle part of the heated zone. Mixtures of CH_4/N_2 or CH_4/H_2 were used as the feed at a total flow of 45 ml/min (STP) for the reactions.

For a reaction, after loading of the catalyst, the reactor was heated at 10 °C/min to the reduction temperature in a gas flow of $H_2:N_2 = 1:3$ or of pure N_2 (in the reaction without reduction). The temperature

was held until the weight of catalyst reached constant. In the constant rate heating reactions, the temperature of the reactor after reduction was lowered to ambient and then it was heated at a rate of 10 °C/min to the reaction temperature in a flow of CH_4:N_2 = 1:2. For the reactions at constant temperatures, after reduction the flow of hydrogen was stopped and the temperature in the reactor was adjusted to the reaction temperature in a flow of nitrogen. Afterwards, methane was switched into the reactor and the reaction began. When the rate of gaining weight approached zero, the flow of methane was stopped while the nitrogen continued to flow until the reactor was cooled to ambient.

3. Results and discussion

3.1. Catalyst characteristics

3.1.1. Specific surface area

BET surface areas of several catalysts used in this work are listed in Table 2. It can be seen that for the catalysts prepared in this work, their specific surface areas are much larger than the results reported previously for the Ni/Al_2O_3 catalyst obtained from co-precipitation [47]. A same phenomenon was observed again that the surface area increases along with the increase of the amount of Al^{3+} contained in the samples. It is shown also that the area reduces with the increase of the calcination temperature for a specific sample, but this effect is not as strong as the effect of the content of the Al^{3+}.

3.1.2. Structure of calcined catalyst

Fig. 1 shows the XRD patterns of the calcined catalyst. Symbol Q1-600 is a Q1 sample calcined at 600 °C. It can be seen that sample Q1-600, which has the lowest Ni/Al ratio among the three samples, contains a γ-Al_2O_3-like phase. $NiAl_2O_4$-like phase is detected in the samples Q2-600 and Q3-600, with Ni/Al ratios of 2:9 and 3:9, respectively. The crystallinity of $NiAl_2O_4$-like spinel phase improves slightly with the increase of the Ni/Al ratio. However, due to the overlaps of the XRD peaks of γ-Al_2O_3 and $NiAl_2O_4$ phases, and the broadened shapes of the peaks in the profiles, this result is only an indication of formation of spinels instead of a single nickel oxide-like phase formed from a hydrotalcite-like precursor [47]. Fig. 2 plots the XRD patterns of sample Q3 calcined at different temperatures. $NiAl_2O_4$-like phase was detected in all the samples irrespective to the calcination temperature. The presence of NiO is not obvious. The crystallinity of $NiAl_2O_4$-like phase becomes better with the increase of the calcination temperature. This preparation method produces $NiAl_2O_4$ spinel-structure in a wide range of calcination temperatures.

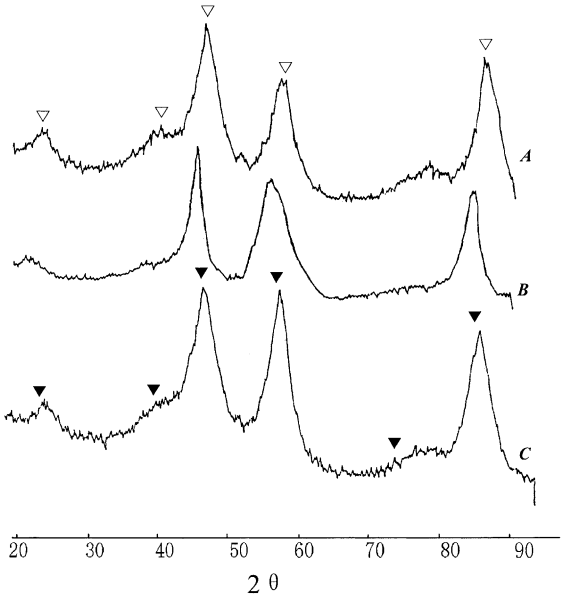

Fig. 1. XRD patterns of catalysts. The peaks of ▼ belong to $NiAl_2O_4$ phase. JCPDS card number 10–339. The peaks of ▽ belong to γ-Al_2O_3. JCPDS card number 29–63. (A) Q1-600; (B) Q2-600; (C) Q3-600.

Table 2
Specific surface areas of samples

Samples	Calcinations temperature (°C)	Surface area (m^2/g)
Q1-600	600	375.00
Q2-600	600	354.94
Q3-400	400	306.73
Q3-500	500	308.50
Q3-600	600	293.95

3.1.3. TPR of mixed oxides

The TPR curve of sample Q3-600 is depicted in Fig. 3. This sample is reduced in two steps. The

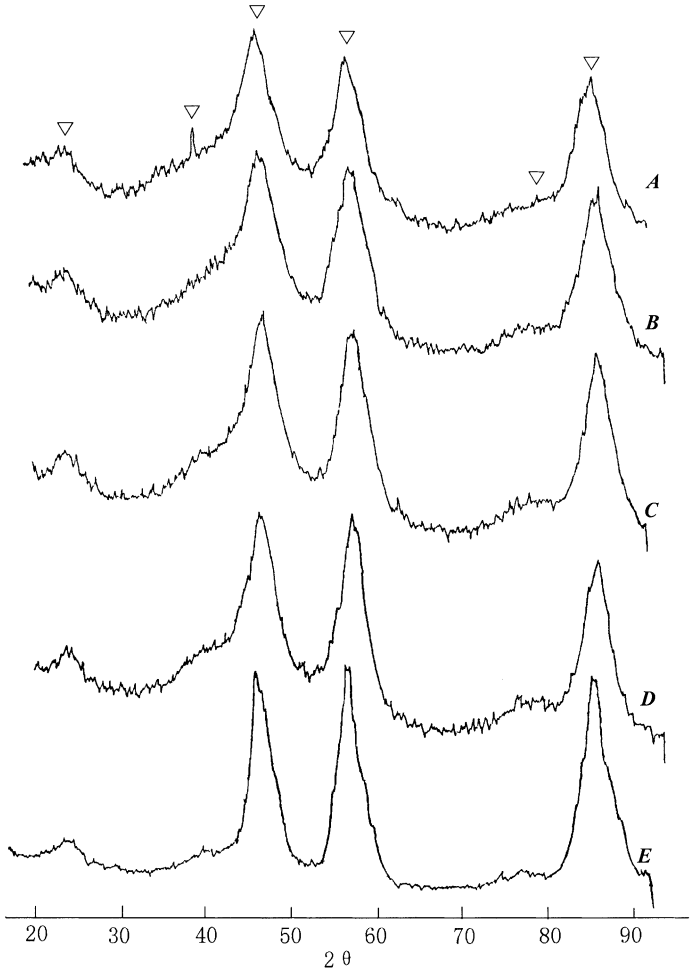

Fig. 2. XRD patterns of Q3 sample calcined at different temperatures. The peaks of ▽ belong to $NiAl_2O_4$ phase. JCPDS card number 10–339. (A) 300 °C; (B) 400 °C; (C) 500 °C; (D) 600 °C; (E) 700 °C.

reduction starts at 349 °C. Up to 524 °C, only a small portion of the nickel is reduced, and a shoulder shaped curve appears in this temperature range. A major peak is observed in 524–904 °C. The reduction completes at 904 °C. This sample completes reduction at a slightly higher temperature than that in [47–49] obtained from a hydrotalcite-like precursor prepared by coprecipitation. This indicates a stronger interaction between nickel and alumina. The small shoulder corresponds to the temperature range of NiO reduction [47,49]. The part of nickel reduced in this range might exist as amorphous or very fine particles of NiO. Its reduction enhances the reduction of the major part of nickel existed in the spinel phase through spillover of hydrogen, and leads to a lower finishing temperature of the reduction peak than expected for a pure spinel phase.

3.1.4. TEM micrograph of catalyst

Fig. 4 shows TEM micrograph of the sample Q3-600 after reduction at 850 °C. It shows that the metal particles are spherically shaped, with diameters in a range of 5–10 nm, and are distributed uniformly on a cotton-like Al_2O_3 matrix. The result shows that

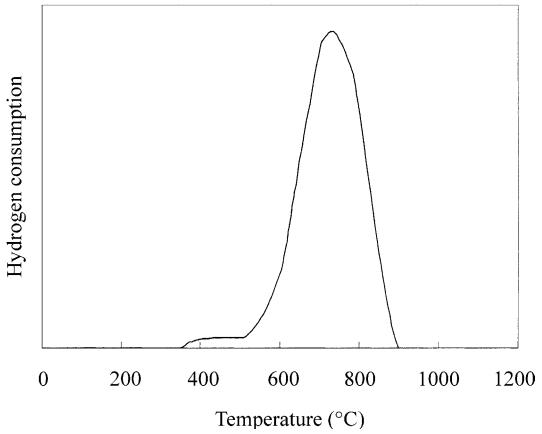

Fig. 3. TPR curve of sample Q3-600.

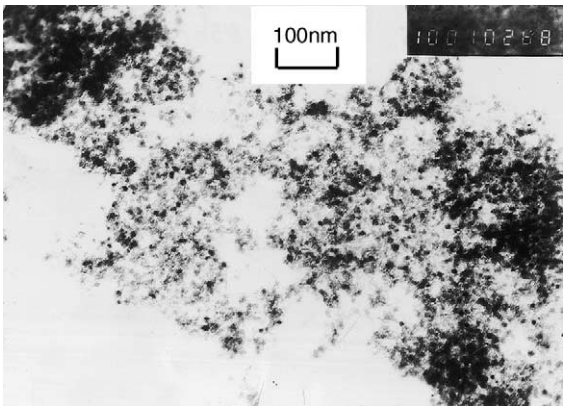

Fig. 4. TEM micrograph of sample Q3-600 reduced at 850 °C.

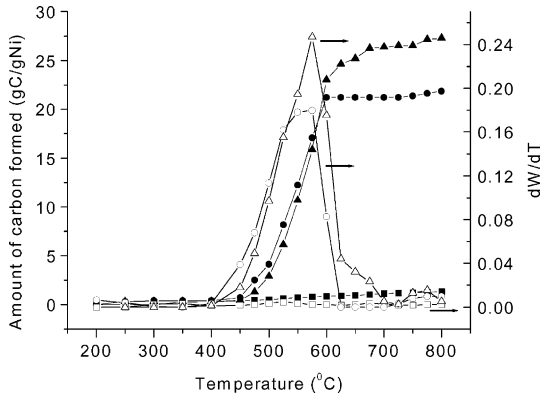

Fig. 5. Amounts and their differential curves of CNTs grown on different catalysts in constant rate heating reactions. ■, □: Q1-600; ●, ○: Q2-600; ▲, △: Q3-600.

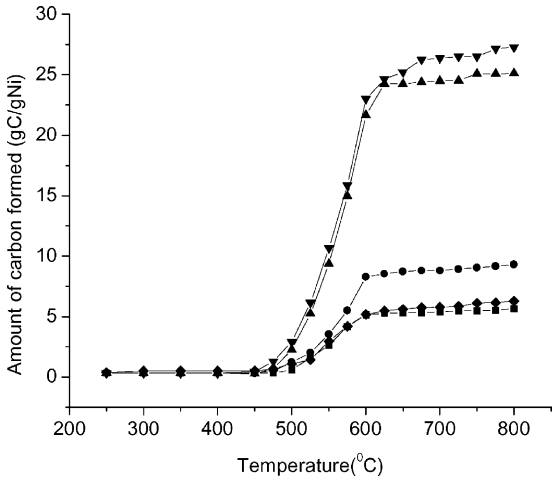

Fig. 6. Amounts of CNT grown on Q3 samples calcined at different temperatures. (■) 300 °C; (●) 400 °C; (▲) 500 °C; (▼) 600 °C; (◆) 700 °C.

nanosized metal particles can be obtained by this method, and furthermore, these particles are likely stable as a result of reduction at the very high temperature.

3.2. Growth of CNT

3.2.1. Results with constant rate heating

Figs. 5 and 6 illustrate the curves of weight gaining process in the constant rate heating reactions and the corresponding differential curves. Both the amount of the carbon formed and the peak height of the differential curve increased with the increase of the Ni content as shown in Fig. 5. There exists an optimum calcination temperature. For the five samples in Fig. 6, the one calcined at 600 °C gives the best performance for carbon growth. The temperature range of CNTs growth for all these catalysts was between 450 and 700 °C.

3.2.2. Effect of conditions on constant temperature reaction

3.2.2.1. Reduction condition. Reduction is one of the important processes which decide the energetic state and the size of the nickel particles in the catalyst.

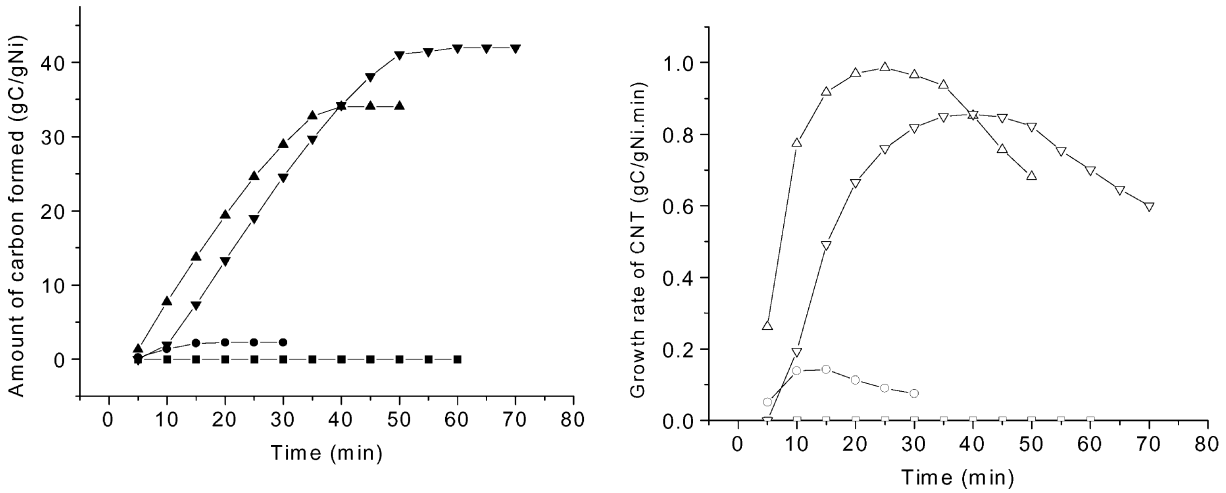

Fig. 7. Rate and amounts of CNT growth on Q3-600 sample reacted at 575 °C with a feed of CH_4:N_2 = 1:2 and reduced with different conditions. □, ■: unreduced; ●, ○: 580 °C; △, ▲: 700 °C; ▽, ▼: 800 °C.

Fig. 7 shows the CNT growing curves at a constant reaction temperature 575 °C on the samples obtained from Q3-600 sample reduced at 580, 700, and 800 °C, respectively. It can be observed that the amount and the rate of CNT growth depend on this factor. It is likely that the overall activity of CNT growth is related to the amount of reduced metallic nickel. Li et al. [47] observed a similar phenomenon with a different catalyst.

3.2.2.2. Reaction temperature. Fig. 8 presents the effect of the reaction temperature on the CNT growth on sample Q3-600. The figure shows that the reaction rate at higher temperatures was faster than that at lower temperatures. However, the catalyst deactivated more rapidly, and as a consequence, the amounts of the CNT formed are smaller at the higher reaction temperatures. Lower temperature favors CNT growth by increasing the possible reaction time, with a compromise

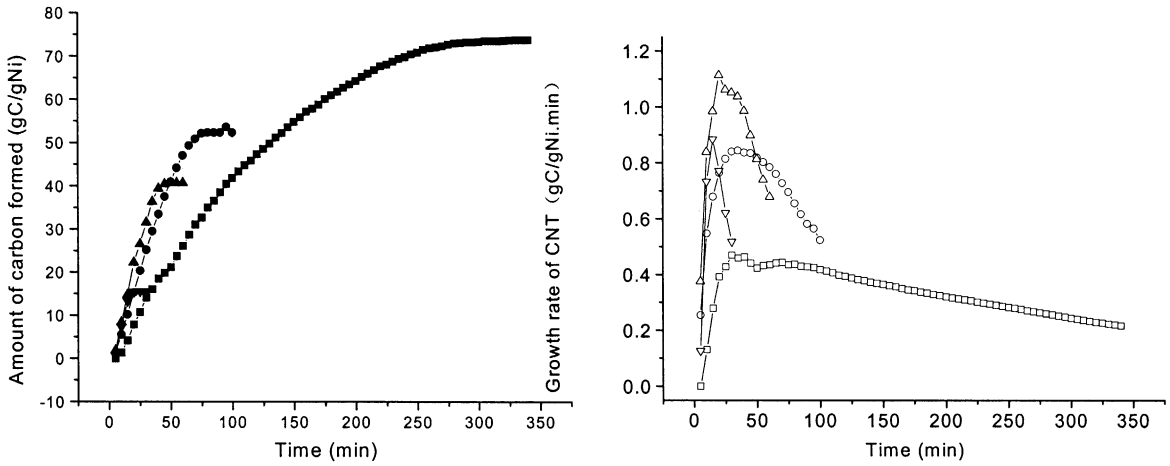

Fig. 8. Amounts and rate of CNT growth on sample Q3-600 reduced at 800 °C and with different reaction conditions. □, ■: 500 °C; ○, ●: 550 °C; △, ▲: 575 °C; ▽, ▼: 600 °C.

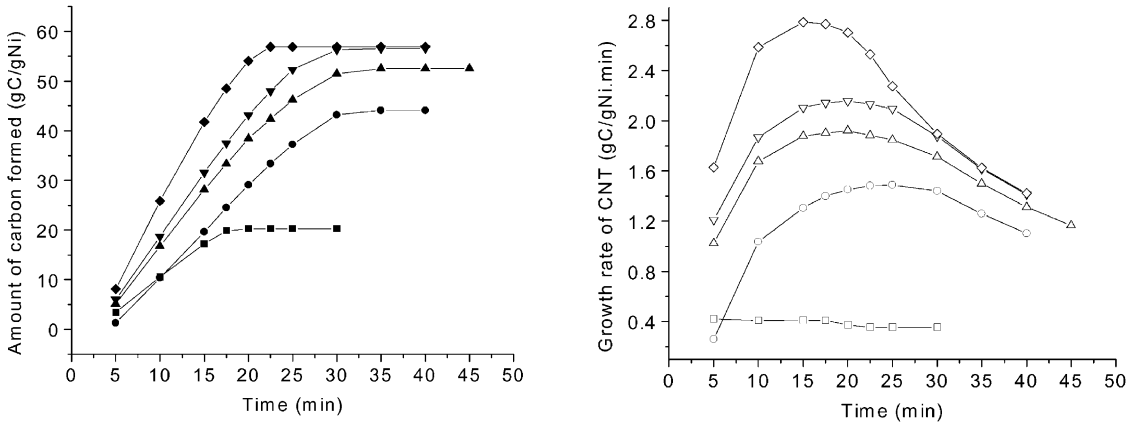

Fig. 9. Amounts and rate of CNT growth on sample Q3-600 with different concentration of methane. Reduction temperature 800 °C and reaction temperature 600 °C. □, ■: 33% CH_4; ○, ●: 50% CH_4; △, ▲: 66% CH_4; ▽, ▼: 75% CH_4; ◇, ◆: pure CH_4.

of a lower reaction rate. In the literature, many results suggest that the amorphous carbon formed when the reaction is too fast encapsulates the active metal and leads to the deactivation and ending of the reaction [48,50,51–54].

3.2.2.3. Feed composition. Fig. 9 represents the effect of the CH_4 concentration in the feed on the reaction. The sample Q3-600 was reduced at 800 °C and the reaction was carried out at 600 °C with mixed methane and nitrogen as the feed. From the figure we can see that, the amount of carbon formed and the growth rate of the CNT increase with the increase of the CH_4 concentration. The weight of CNT grown in the pure methane reaches as high as 56.9 g C/g Ni.

Figs. 10 and 11 depict the effect of the dilution gases, here H_2 or N_2, on the CNT growth. The other conditions were the same as that of Fig. 9, while the gases CH_4:H_2 = 1:2, 2:1 or that CH_4:N_2 = 1:2, 2:1 were used. Fig. 10 shows that the catalyst has no activity with CH_4:H_2 = 1:2 at the specific reaction temperature, but its activity is rather high when CH_4:N_2 = 1:2 was used. From Fig. 11 it is obvious that the amount of the CNT grown and the time pe-

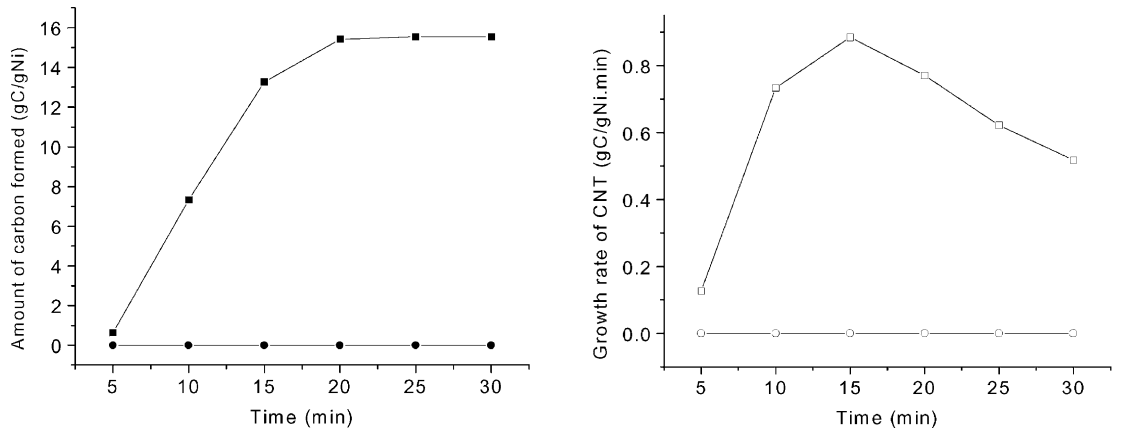

Fig. 10. Rate and amounts of CNT growth on sample Q3-600 with different dilution gas. Reduction temperature 800 °C and reaction temperature 600 °C. □, ■ CH_4:H_2 = 1:2; ○, ● CH_4:N_2 = 1:2.

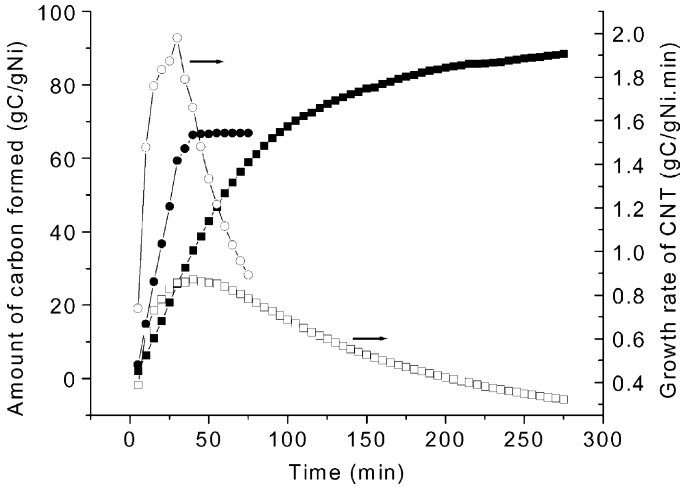

Fig. 11. Rate and amounts of CNT growth on sample Q3-600 with different dilution gas. Reduction temperature 800 °C and reaction temperature 600 °C. □, ■ CH_4:H_2 = 2:1; ○, ● CH_4:N_2 = 2:1.

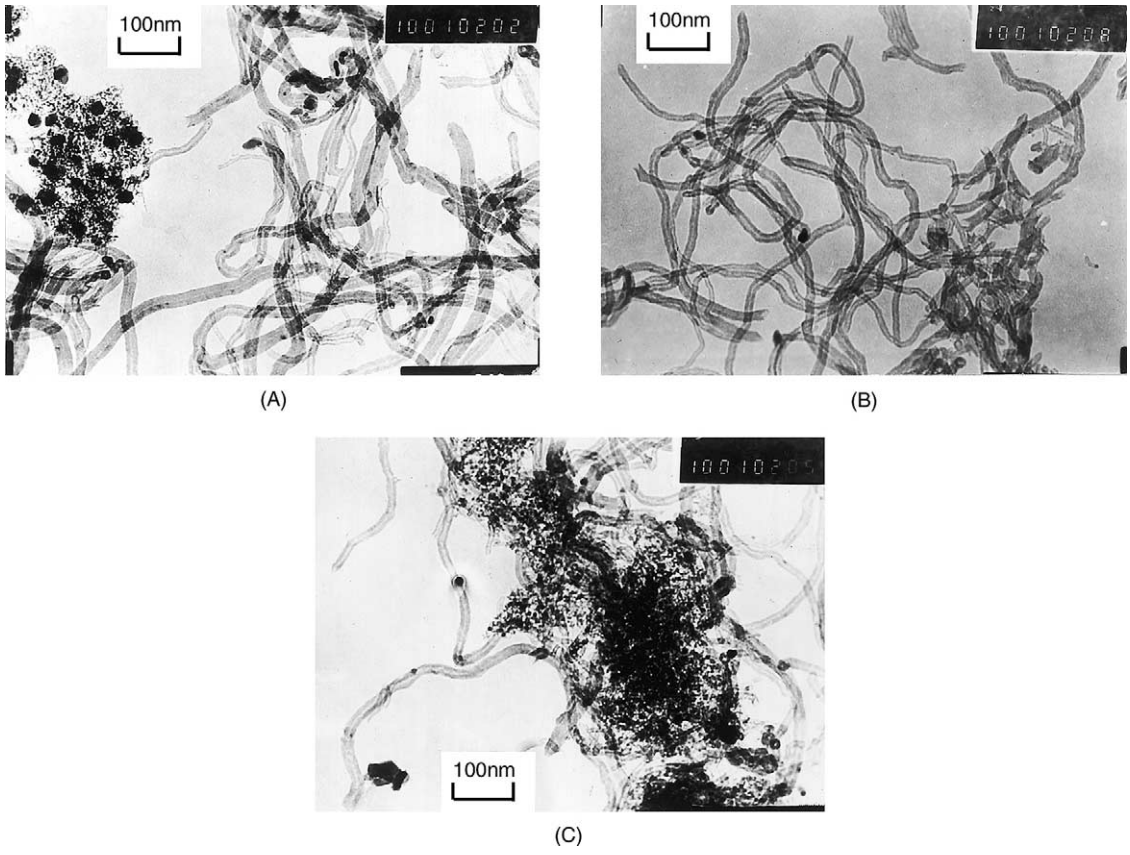

Fig. 12. TEM micrographs of CNT grown on Q3-600 sample reduced at 800 °C and reacted at different temperatures: (A) formed at 500 °C; (B) formed at 550 °C; (C) formed at 575 °C.

riod of the activity with H_2 as dilution gas were better, however, the rate was lower, than that with N_2. The presence of hydrogen retards evidently the MDR, because it is one of the products. This has a good effect if the temperature is suitable. It prolongs the reaction time, lowers the rate of the deactivation, and, as a consequence of a smooth growing, leads to the formation of a large amount of CNTs. Many publications reported using hydrogen as a dilution gas of methane for CNT growth over group VIII metals, and proposed that hydrogen lowers the rate of carbon formation and prevents the catalyst particles from being encapsulated [51,55–58].

It should be noted that an induction period less than 5 min might exist for each reaction when methane and nitrogen mixture was used as the feed. However, the volume of the tubing was not precisely calibrated.

3.3. Morphology of as-grown CNT

3.3.1. Effect of reaction temperature

Fig. 12 shows the TEM micrographs of the CNTs grown on sample Q3-600 at reaction temperatures of 500, 550 and 575 °C, respectively. The other conditions were the same for all the samples as: reduction temperature 800 °C, feeding composition CH_4:N_2 = 1:2. All the CNTs in the three images are curved and hollow tubes. The diameters of the CNTs are similar to that of the catalyst particles on their tips. In image A, the diameters of the CNTs are in the range of 10–20 nm and the thickness of the walls is in the range of 5–10 nm. There exist some spherical catalyst particles inactive for the CNT's growth, with diameters in a range of 15–30 nm. In image B and C, the diameters of the CNTs are around 10 nm and the thickness

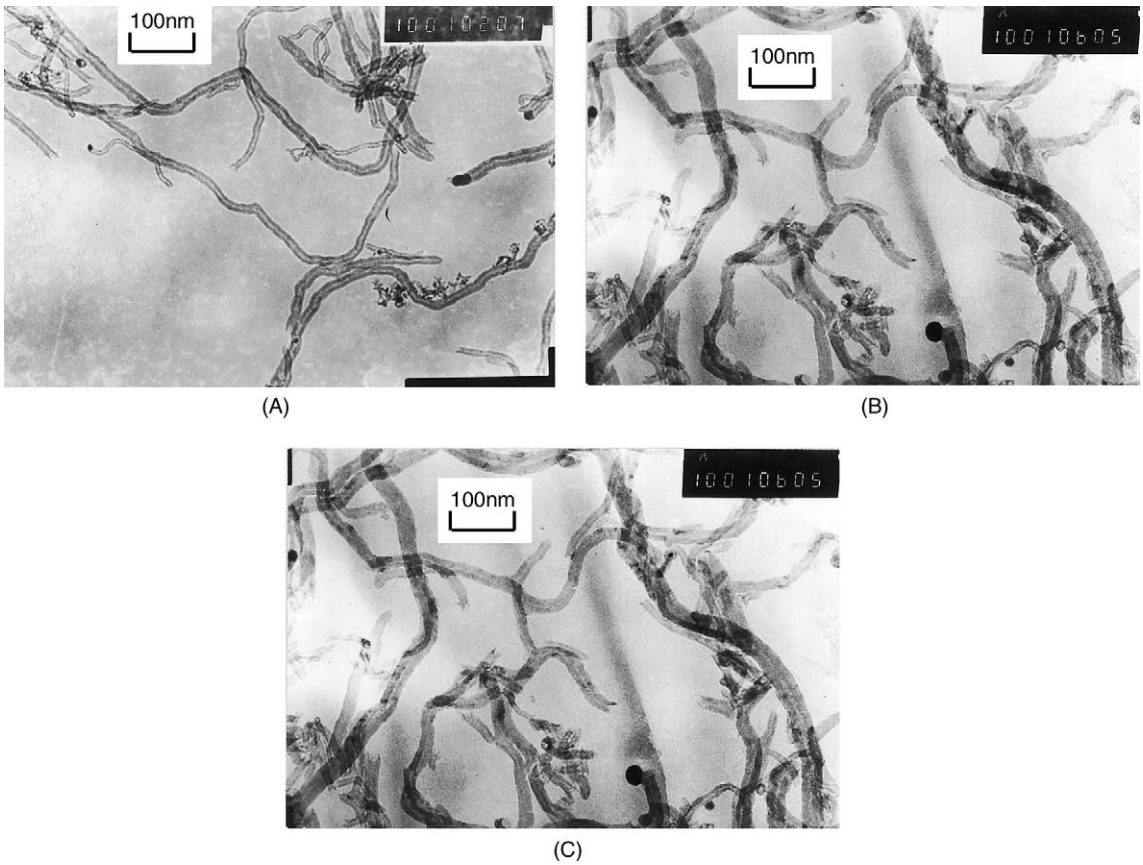

Fig. 13. TEM micrographs of CNTs grown on Q3-600 sample reduced at 800 °C and reacted at 600 °C with different methane concentration: (A) CH_4:N_2 = 1:2; (B) 2:1; (C) pure methane.

of the walls is in the range of 2–5 nm. The diameters and widths of the walls of the CNTs become thinner with the increase of the reaction temperature.

3.3.2. Effect of methane concentration

Fig. 13 shows the TEM micrographs of the CNTs obtained with different methane concentration in the feed. The reduction temperature of the catalyst was 800 °C and the reaction temperature was 600 °C. The diameters and the wall widths of the CNTs in image A are around 10 and 3 nm, respectively. Image B shows that the CNTs have larger diameters and thicker walls, in the ranges of 15–20 and 3–8 nm, respectively. In image C the CNTs show a further thicker feature than those in image A and B. The morphology of the CNTs becomes more complex and their diameters become larger with the increase of the methane concentration.

The following several common features were noticed from these and other TEM observations: (1) The CNTs grown on the catalyst in this work seem to be thinner than those obtained on the coprecipitated catalyst reported previously [5,19,20,47,58]. (2) CNTs show hollow and curved structures with smooth and regular internal and outer surfaces, indicating no gas phase deposition of carbon on the outer surface of the CNTs. (3) The morphology of the CNTs is rather unique for a specific reaction. (4) The size of the catalyst particles is similar to the diameter of the CNTs. (5) The break sections of the CNTs have male and female conic shapes, favoring the fishbone structure model rather than the layered annular tube model of the CNT structure [59–61]. (6) The existence of a distribution of the CNTs' diameters indicates the presence of a size distribution of the catalyst particles, which was determined by the preparation, reduction and the reaction conditions in the induction period.

4. Conclusions

The sol–gel and subsequent supercritical drying method favors the formation of spinel-structured $NiAl_2O_4$ or γ-Al_2O_3 phases in a wide range of calcination temperature. The catalysts prepared with this method have a large surface area, high porosity and ultra-low-density. After reduction, nanosized metal catalyst can be obtained.

The amount of the CNTs formed in MDR increases with the amount of nickel in the catalyst. The temperature range for CNTs growth for all the catalysts was between 450 and 700 °C. The catalyst reduction and MDR reaction conditions, and the feed composition all have a profound effect on the MDR. A higher reaction temperature leads to a higher reaction rate and a quick deactivation of the catalyst. The amount of carbon formed, and the time period of activity increased with the increase of the reduction temperature. The amount and the rate of CNT growth increased with the increase of the CH_4 concentration. The presence of hydrogen retards the MDR. However, the hydrogen has some positive effect on the growth of the CNT by prolonging the reaction time.

The morphology of the CNTs illustrates that the CNTs formed under these conditions have a curved, hollow, and tubular shape, with diameters in the range of 10–20 nm. The break sections have both male and female conic shapes, which favors the fishbone structure model of the carbon. Both reaction and the reduction conditions have influence on the morphology of the CNTs. The diameters of the CNTs are similar to the sizes of the catalyst particles. The existence of the distribution of the diameters of CNTs indicates that the presence of a distribution of the catalyst particle size, which was determined by preparation and reaction conditions of the induction period.

Acknowledgements

The financial support from a 973 Program of the Chinese Ministry of Science and Technology under contract number G-199902240 and from NSF of China under contract numbers 20006072, 29792079-2 and 29876032 are gratefully acknowledged.

References

[1] S. Iijima, Nature 354 (1991) 56.
[2] A. Maiti, C.J. Brabec, C.M. Rol, J. Bernhole, Phys. Rev. Lett. 73 (1994) 2468.
[3] S. Seraphin, D. Zhou, Appl. Phys. Lett. 64 (1994) 2087.
[4] K. Hernadi, A. Fonseca, J.B. Nagy, A. Siska, I. Kiricsi, Appl. Catal. A 199 (2000) 245.
[5] Y.D. Li, J.L. Chen, Y.N. Qin, L. Chang, Energ. Fuels 14 (2000) 6.

[6] J. Vilcakova, P. Saha, V. Kresalek, O. Quadrat, Synth. Met. 113 (2000) 83.
[7] K. Kaneto, M. Tsuruta, G. Sakai, W.Y. Cho, Y. Ando, Synth. Met. 103 (1999) 2543.
[8] A.C. Dillon, K.M. Jones, T.A. Bekkkedahl, C.H. Kiang, D.S. Bethune, M.J. Heben, Nature 386 (1997) 377.
[9] X.B. Wu, P. Chen, J. Lin, K.L. Tan, Int. J. Hydrogen Energ. 25 (2000) 261.
[10] B. Coq, J.M. Planeix, V. Brotons, Appl. Catal. A 173 (1998) 175.
[11] N.M. Rodriguez, M.S. Kim, R.T.K. Baker, J. Phys. Chem. 98 (1994) 13108.
[12] S. Amelinckx, D. Bernaerts, X.B. Zhang, G. van Tendeloo, J. van Landuyt, Science 267 (1995) 1334.
[13] Y. Saito, T. Yoshikawa, M. Inagaki, Chem. Phys. Lett. 204 (1993) 277.
[14] T. Guo, P. Nikolaev, A. Thess, Chem. Phys. Lett. 260 (1996) 471.
[15] D.T. Colbert, R.E. Smalley, Chem. Phys. Lett. 243 (1995) 49.
[16] V. Ivanov, J.B. Nagy, Ph. Lambin, A. Lucas, X.B. Zhang, X.F. Zhang, D. Bernaerts, G. van Tendeloo, S. Amelinckx, J. van Landuyt, Chem. Phys. Lett. 223 (1994) 329.
[17] M. Ishioka, T. Okada, K. Matsubara, Carbon 30 (1992) 859.
[18] M. Ishioka, T. Okada, K. Matsubara, Carbon 30 (1992) 865.
[19] J.L. Chen, Y.D. Li, M.Y. Mei, Y.N. Qin, L. Chang, Carbon 39 (2001) 1467.
[20] Y.D. Li, J.L. Chen, Y.M. Ma, J.B. Zhao, Y.N. Qin, L. Chang, Chem. Commun. (1999) 1141.
[21] T.W. Ebbesen, P.M. Ajayan, Nature 358 (1992) 220.
[22] C.N.R. Rao, R. Seshadri, R. Sen, A. Govindaraj, Mater. Sci. Eng. B 15 (1995) 209.
[23] S. Iijima, T. Ichihashi, Nature 363 (1993) 603.
[24] D.S. Bethune, C.H. Kiang, M.S. de Vries, G. Gorman, R. Savoy, J. Vasquez, R. Beyers, Nature 363 (1993) 605.
[25] C.H. Kian, W.A. Goddard Go III, R. Beyers, J.R. Sslem, D. Bethune, J. Phys. Chem. Solids 57 (1996) 35.
[26] C.G. Plecourt, Y. Le Bouar, A. Loiseau, H. Pascard, Nature 372 (1994) 761.
[27] C. Journet, W.K. Maser, P. Bernier, A. Loiseau, M. Lamy de la Chapelle, S. Lefrant, P. Deniard, R. Lee, J.E. Fisher, Nature 388 (1997) 756.
[28] T. Guo, P. Nikolaev, A. Thess, D.T. Colbert, R.E. Smalley, Chem. Phys. Lett. 243 (1995) 49.
[29] A. Thess, R. Lee, P. Nikolaev, H. Dai, P. Petit, J. Obert, C. Xu, Y.H. Lee, S.G. Kim, A.G. Rinkler, D.T. Colbert, G.E. Scuseria, D. Tomanek, J.E. Fisher, R.E. Smalley, Science 273 (1996) 483.
[30] M.S. Dresselhaus, G. Dresselhaus, K. Sugihara, I.L. Spain, H.A. Goldberg, Graphite Fibers and Filaments, Springer, Berlin, 1988.
[31] H. Dai, A.G. Rinzler, P. Nikolaev, A. Thess, D.T. Colbert, R.E. Smalley, Chem. Phys. Lett. 260 (1996) 471.
[32] R.T.K. Baker, P.S. Harris, R.B. Thomas, R.J. Waite, J. Catal. 30 (1993) 86.
[33] S. Amelinckx, X.B. Zhang, D. Bernaerts, X.F. Zhang, V. Ivanov, J.B. Nagy, Science 265 (1995) 635.
[34] K. Hernadi, A. Fonseca, J.B. Nagy, D. Bernaerts, A. Fudala, A.A. Lucas, Zeolites 17 (1996) 416.
[35] M. Su, B. Zheng, J. Liu, Chem. Phys. Lett. 322 (2000) 321.
[36] J.B. Donnet, Carbon Black, Marcel Dekker, New York, 1976, p. 16.
[37] J.B. Pohleny, N.H. Scott, US Patent 3 284 161 (1996), to Universal Oil Products.
[38] M. Steinberg, H.C. Cheng, Int. J. Hydrogen Energ. 14 (1989) 797.
[39] N.Z. Muradov, Int. J. Hydrogen Energ. 18 (1993) 211.
[40] T. Zhang, M.D. Amiridis, Appl. Catal. A 167 (1998) 161.
[41] R. Aiello, J.E. Fiscus, H.C.Z. Loye, M.D. Amiridis, Appl. Catal. A 192 (2000) 227.
[42] S. Takenaka, H. Ogihara, I. Yamanaka, K. Otsuka, Appl. Catal. A 217 (2001) 101.
[43] M.A. Ermakova, D.Y. Ermakov, A.L. Chuvilin, G.G. Kuvshinov, J. Catal. 201 (2001) 183.
[44] B. Monnerat, L. Kiwi-Minsker, A. Renken, Chem. Eng. Sci. 56 (2001) 633.
[45] K. Otsuka, S. Kobayashi, S. Tatenaka, Appl. Catal. A 210 (2001) 371.
[46] T.V. Choudhary, C. Sivadinarayama, C.C. Chusuei, A. Klinghoffer, D.W. Goodman, J. Catal. 199 (2001) 9.
[47] Y.D. Li, J.L. Chen, L. Chang, Appl. Catal. A 163 (1997) 45.
[48] Y.D. Li, J.L. Chen, L. Chang, J.S. Zhao, Stud. Surf. Sci. Catal. 118 (1998) 321.
[49] J.L. Chen, Study on the production and utilization of carbon nanofibers from catalytic decomposition of methane, Thesis, Tianjin University, 1999.
[50] D.L. Trimm, Catal. Rev. Sci. Eng. 16 (1977) 155.
[51] J.R. Rostrup-Nieslen, J. Catal. 127 (1972) 343.
[52] J.R. Rostrup-Nieslen, D.L. Trimm, J. Catal. 48 (1977) 155.
[53] R.T.K. Baker, M.A. Barber, P.S. Harris, F.S. Feates, R.J. Waite, J. Catal. 26 (1972) 51.
[54] G.G. Tibbetts, J. Cryst. Growth 66 (1984) 632.
[55] N.M. Rodriguez, J. Mater. Res. 8 (1993) 3233.
[56] F. Benissad, P. Gadelle, M. Coulon, L. Bonnetain, Carbon 26 (1988) 61.
[57] F. Benissad, P. Gadelle, M. Coulon, L. Bonnetain, Carbon 27 (1989) 585.
[58] Y.D. Li, J.L. Chen, L. Chang, Y.N. Qin, J. Catal. 178 (1998) 76.
[59] M. Hoogenraad, The growth and utilization of carbon fibrils, Thesis, University of Utrecht, 1995.
[60] G.G. Tibbetts, Appl. Phys. Lett. 42 (1983) 666.
[61] G.G. Tibbetts, J. Cryst. Growth 66 (1984) 632.